2000

Astronomical hyperspectral imaging flatfield corrections

Katherine Hoheusle

SIMG-503
Senior Research

Astronomical Hyperspectral Imaging
Flatfield Corrections
Final Report

Katherine T. Hoheusle
Center for Imaging Science
Rochester Institute of Technology
October 2000

Table of Contents

Astronomical Hyperspectral Imaging

Katherine T. Hoheusle

Table of Contents

[Title Page](#)

Astronomical Hyperspectral Imaging

Katherine T. Hoheusle

Abstract

Using observations of data acquired through a tunable, liquid-crystal filter of the central region of the Jewel Box cluster, NGC4755, a tunable, liquid-crystal filter was tested to see how well low-resolution spectrophotometry of multiple stars within a moderately crowded field could be performed. To evaluate the filter, the filter's central wavelength was stepped from 435 nanometers (nm) to 720 nm in successive intervals of 5 nm. Given the limited telescope time, the flatfield data obtained was stepped in intervals of 50 nm. Zoran Ninkov, Robert Slawson and Elliott Horch, the three RIT faculty/staff members working in the project, assumed that it would be possible to adequately correct the data for spatial transmission using such widely spaced flatfield images. After reviewing this data, it was found that this belief was in error.

The mission of this Senior Research Project therefore was:

- Examine the magnitude of the flatfielding errors in different regions of the data field;
- Test whether or not data corrected with flatfield images obtained in the laboratory rather than at the telescope improved the data analysis;
- To see how well the spectral extracted for a few stars in the cluster, with known spectral type agreed with the expected spectra from a standard atlas (i.e. Gunn & Stryker).

Table of contents

This report is accepted in partial fulfillment of the requirements of
the course SIMG-503 Senior Research.

Title: Astronomical Hyperspectral Imaging: Flatfield Corrections

Author: Katherine T. Hoheusle

Project Advisor: Zoran Ninkov, PhD

SIMG-503 Instructor: Joseph P. Hornak

Table of Contents

Astronomical Hyperspectral Imaging
Katherine T. Hoheusle

Acknowledgement

I would like to acknowledge the following people for their contributions:

Zoran Ninkov, PhD……Faculty Advisor

Robert Slawson, PhD…….Co-Advisor

Albert Piterman, Graduate Student Assistant……Laboratory Simulations

Table of Contents

Astronomical Hyperspectral Imaging
Katherine T. Hoheusle

Background:

Robert Slawson, Zoran Ninkov, and Elliott Horch published a paper in 1999 titled "Hyperspectral Imaging: Wide-Area Spectrophotometry Using A Liquid-Crystal Tunable Filter[1]." The objective of the study was "to report on the use of the tunable, liquid filter to obtain simultaneous, low-resolution spectrophotometry of multiple stars within a moderately crowded field[1]
" by analyzing data of the stellar cluster, NGC 4755, also known as the Jewel Box cluster, Figure 1. The cluster is named for its one red (κ
Crucis) and four blue supergiant stars. This star cluster was picked because some of the stars in the field had already known spectral types used as reference spectra and as a result could be used for independent confirmation of spectral type in the research done. These reference spectra were used for comparison with already established atlas values from Gunn & Stryker publications[2]. In this paper, star I-15, with the spectral type B1-V according to Gunn & Stryker[2], was selected as the fundamental reference star for the cluster.

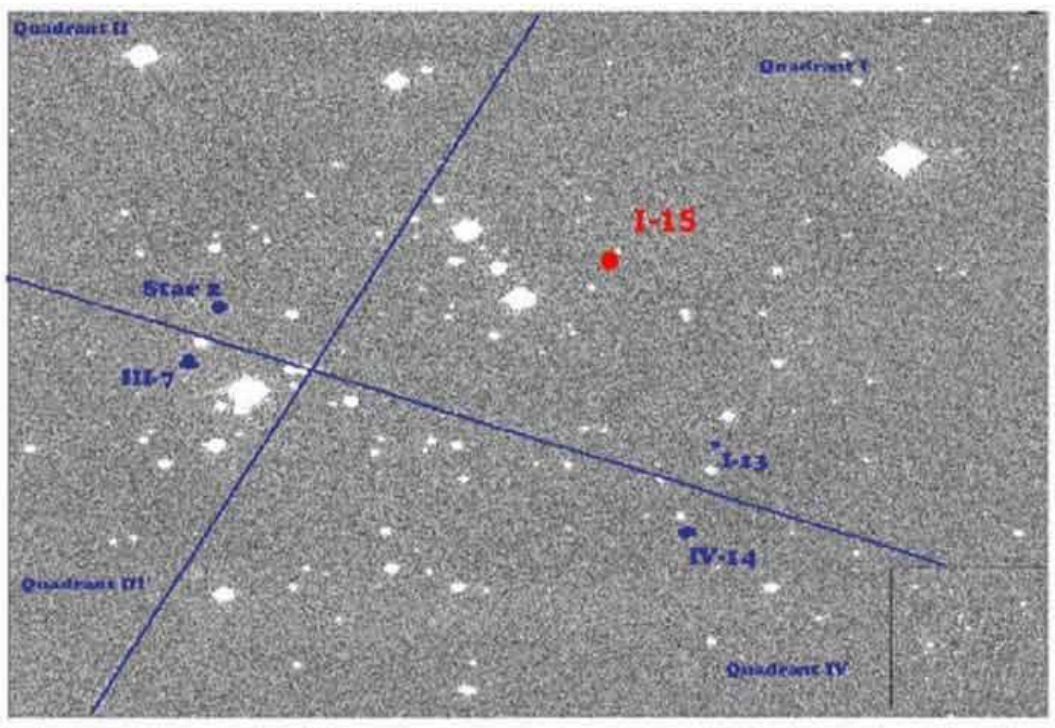

Figure 1: Central Region of NGC 4755, "Jewel Box Cluster" with Reference Star I-15 at 590 nm with astronomical North at 15 degrees clockwise from the top and astronomical East at 15 degrees clockwise from the left

Slawson, Ninkov and Horch captured images of the NGC4755 at wavelengths over the range 435 nm to 720 nm. The imaging system they used is listed below;

- Las Campanas Observatory in Las Campanas, Chile
- 61 cm Cassegrain telescope, courtesy of the University of Toronto, Canada
- Varispec VIS2-10 Liquid Crystal Tunable Filter, housed in a 7.5 x 7.5 x 4 cm aluminum case
    - This is a multistage Lyot-Ohman type polarization interference filter.
- Kodak KAF-4200 2048 x 2048 CCD camera with 9 μm square pixels
    - The CCD chip was housed in a Photometrics CH-250 camera cooled to -35^{o} C using a thermoelectric cooler and cooled circulating water.

Fully assembled, the basic imaging system is illustrated in Figure 2, as shown below:

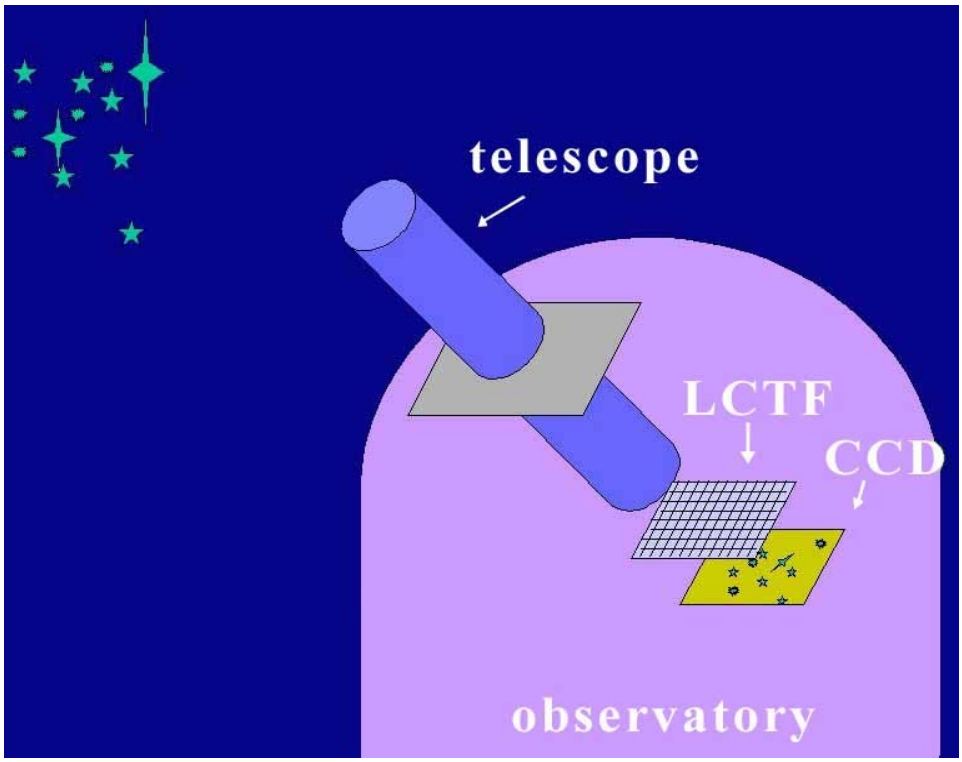

Figure 2: Simplified set up of the imaging system apparatus

The liquid crystal tunable filter, a multistage Lyot-Ohman type polarization interference filter[4] with an added liquid-crystal waveplate in each stage, provides an electronically controllable variable retardance. An illustration of a single Lyot-Ohman cell is shown in Figure 3. When a voltage is applied across the two electrodes that are in the liquid crystal waveplate, an E-field parallel to the light path is induced. This is a torque that is exerted on the polar liquid crystal molecules and results in twisting them into the direction of the E-field.

Because of this twisting motion, the molecules align more closely with the applied field and the retardance through the liquid-crystal waveplate decreases. The result is a waveplate with an electronically adjustable retardance. This is the basic mechanism by which wavelength tunability is achieved.

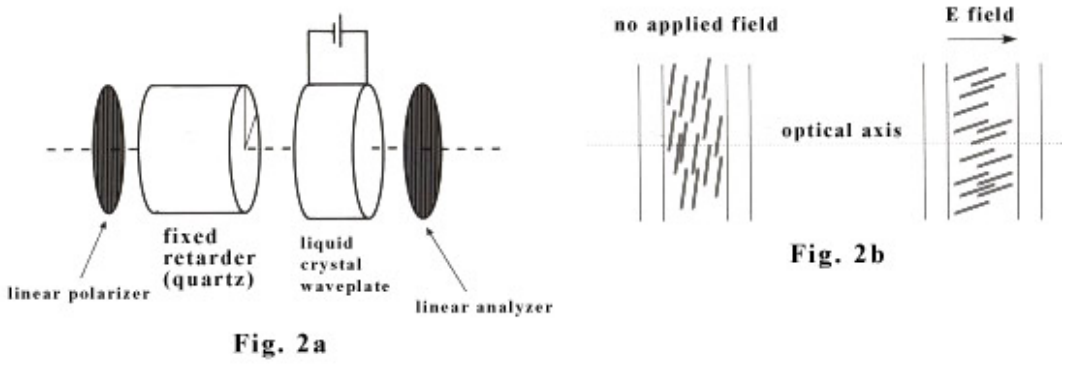

Figure 3: Schematic diagram of a single Lyot-Ohman cell[1]

The wavelengths were scanned, using the apparatus being tested, in increments of 50 nm, increasing from 435 nanometers to 720 nanometers. From the collected data, Slawson, Ninkov and Horch were able to obtain the spectrum for five of the brightest stars in the cluster by normalizing the flux for a single star in each reference frame to its known spectral energy distribution points. Differential corrections were determined by using a standard spectral scan for a reference star with a known spectral type, in this case, Star I-15. Dereddened spectra were constructed using the reference star as a guide. Uncertainties were based on expected variable reddening across the cluster.

After as much data as possible was collected from the observatory, the images were processed using a standard IRAF CCD processing pipeline, trimmed, bias subtracted and flat-fielded to generate calibrated data. Once this was done, all of the frames were aligned to a common pixel coordinate system and conceptually stacked into a data cube with the axes consisting of X-Y planes (image) and wavelength (nm, spectral) axes.

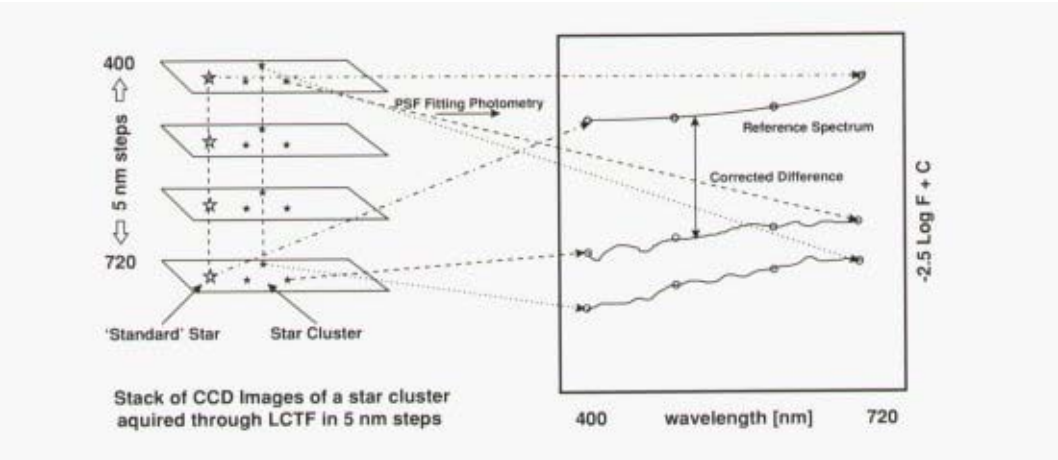

Figure 4: Illustration of Hyperspectral stacking of cluster images by extraction of continuum scans[1]

My original focus was to expand the research done in the Slawson, Ninkov and Horch paper, which consisted of the analysis of five stars, to as many stars in the NGC 4755 star cluster from the same data. This analysis would in turn identify what kind of stars are in the cluster based on their spectra. The compiled results would be turned into an interactive web tool that would make obtaining information on different stars in the cluster more convenient. If the method used in this study proved to be effective time wise and accurate, then this method could be applied to other star clusters astronomers are currently and planning to study in order to make a convenient star catalog easily accessible by the touch of a mouse.

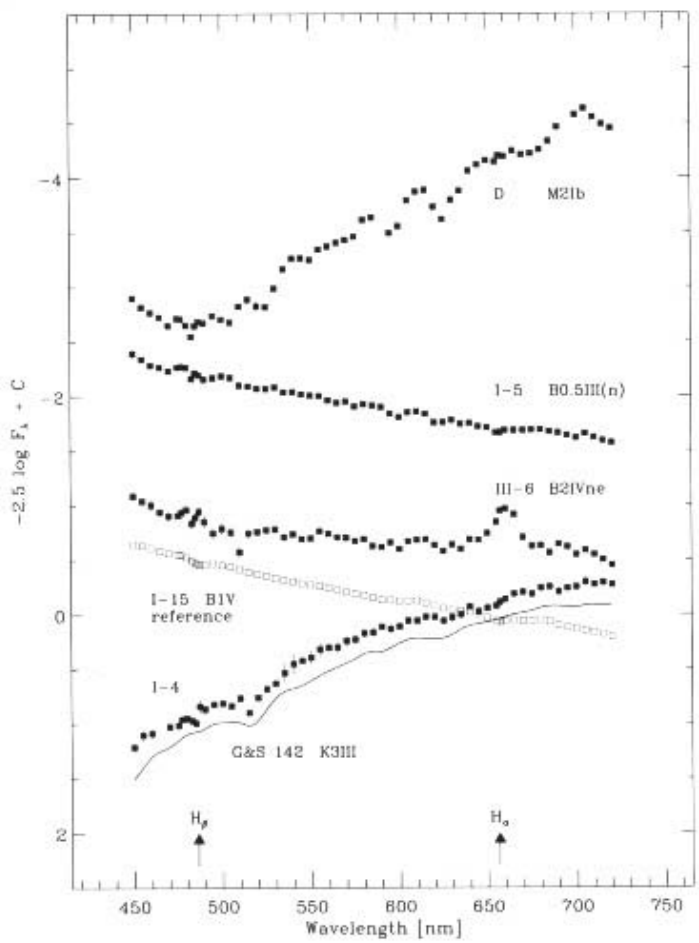

Figure 5: Spectral Graph of Analysis of the Original Five Stars in the Study[1]

However, during the past academic year of 1999-2000, the original research team, along with graduate student assistant Albert Piterman, and undergraduate student assistant, Katherine Hoheusle (me), both students at the Chester F. Carlson Center for Imaging Science on the Rochester Institute of Technology campus, discovered previously undetected errors in the study. The original spectral analysis of the five stars in the study, shown in Figure 5: I-13 in Quadrant 1, Star 2 in Quadrant 2, III-7 in Quadrant 3 and IV-14 in Quadrant 4, turned out to be calibrated incorrectly due to insufficient flatfield data collected during the allocated observatory time at the Las Campanas Observatory.

At this point, my Senior Project changed in focus. My goal became to take the stars that had been classified as BI-V stars in the cluster from previous studies and see if the reduced spectral energy distribution compiled through the experimental tunable, liquid-crystal filter and subsequent algorithms matched the Gunn & Stryker[2] stellar atlas descriptions. If these stars matched, then it would provide confidence that the new tunable, liquid-crystal filter worked.

Theory:

The test images were obtained in February of 1997 using the liquid-crystal tunable filter at the Las Campanas

Observatory in the Chilean Andes Mountains on the South American continent. One requirement in order to calibrate the system effectively was to take flatfield images of the interior white dome at different wavelengths between 435 nm and 720 nm
in order to quantify spatial sensitivity variations of the imaging system. To save time and disk space, the wavelength intervals between consecutive flatfield measurements were increased from the proposed 5 nm to 50 nm. It was believed that this would not make a significant difference to the final results using the experimental tunable, liquid-crystal filter.

When the results were again analyzed in Rochester, NY later in 1999, the team found that this approach was not effective. In turn, the results they published were not as accurate as they had originally expected. Given an ideal situation, there would be no spatial variations in sensitivity of the filtered imaging system taken in increments of 50 nm
and therefore a ratio of one should be expected between two flatfield images of successive wavelength measurements. In theory, an image at 580 nm could be flattened with a flatfield image at 600 nm while the image at 570 nm could be flattened with a flatfield image at 550 nm.

However, the team found that the transmission through the filter had spatial variations that changed with wavelength setting, as is visually apparent from the boxes in Figure 6a, thus the flattened image at 600 nm did not correctly flatten the data at 580 nm. The same thing happened for data at 570 nm flattened by the flatfield image at 550 nm. As a result, the ratio of the flatfield at 650 nm to 600 nm
resulted in a graph that deviated significantly from one, as shown in Figure 6b.

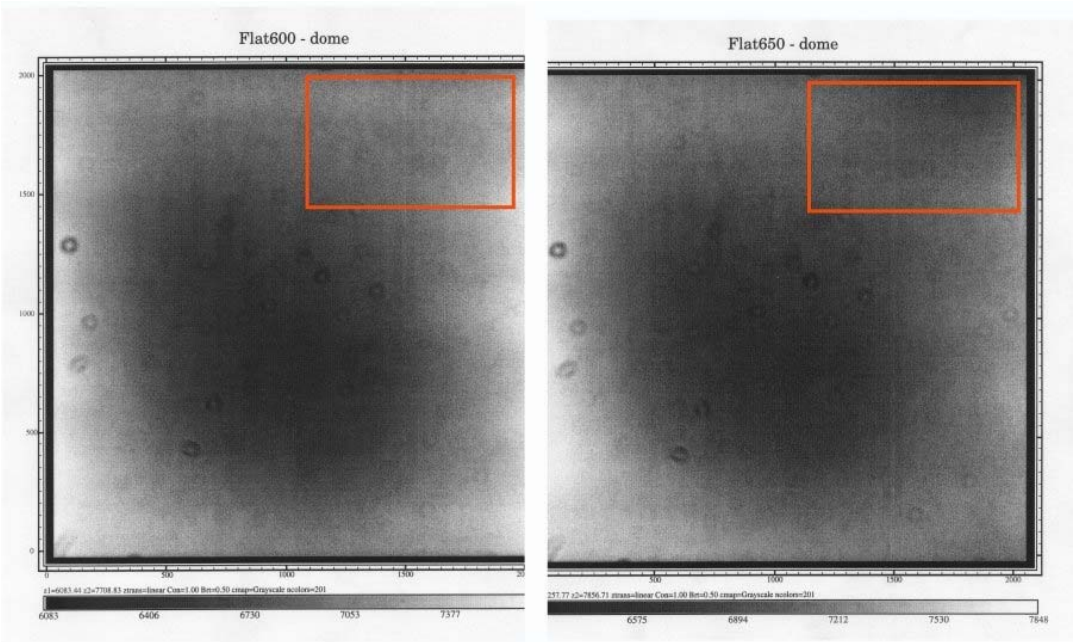

Figure 6a: Original Flatfields at 600 nm and 650 nm

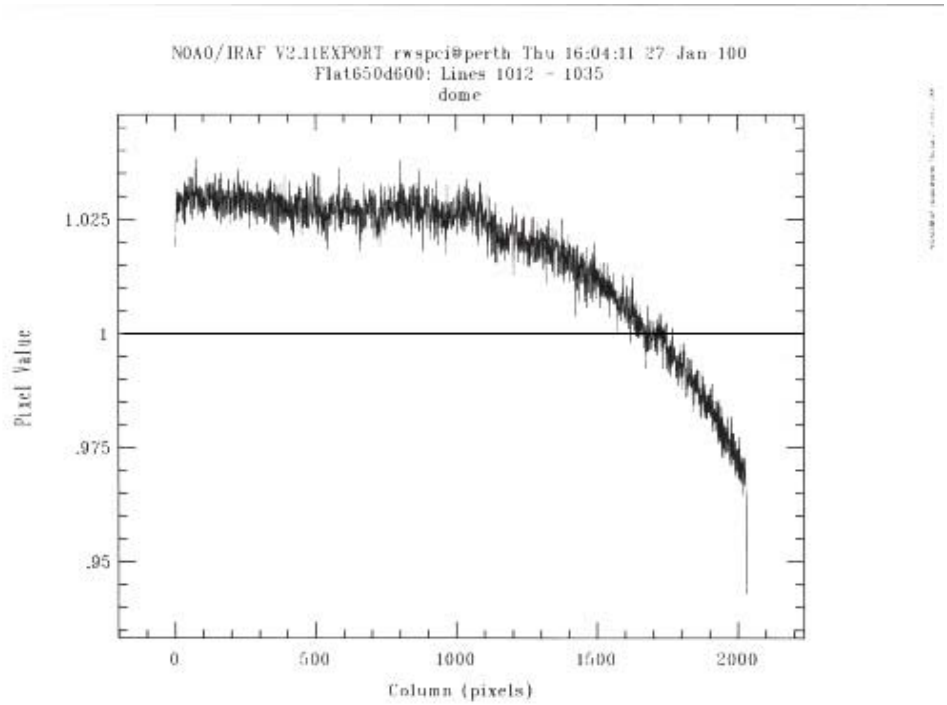

Figure 6b: Ratio of flatfield at 650 nm and 600 nm Average of lines 1012-1035

Given this new information, the team found that in order to get accurate data, the flatfield measurements needed to be re-done by using algorithms that averaged out the measured data from the observatory along with new measurements done in the laboratory.

To find the correct flatfield calibrations, reference spectral graphs from research done by Gunn and Stryker's[2] experiments of the same type of star, BI-V, were utilized to compare the results of the original set of flatfield values with results of the new set of flatfield values , which were obtained through using the liquid crystal tunable filter in a laboratory setting that simulated the observatory white walls in order to completely measure the sensitivity of the filter at different wavelengths using a large number of much smaller intervals between 400 nm and 720 nm, Figure 9.

At the time of the publication of the paper, the team believed that the dome flatfield corrections were not optimal, resulting in an estimated uncertainty of approximately 1.4 percent in the final photometry.

Methods:

In order to convert the raw data obtained by the imaging system into useful data that could be interpreted, specific steps had to be followed. First, bias was subtracted from the raw data and then the flatfielded image at the closest wavelength was divided into this difference. The result was a calibrated image where the relative brightness ratio was preserved. The spectral energy distribution of any star in turn could be interpreted as a specific type of star based on the continuum and spectral characteristics using a stellar reference guide such as Gun & Stryker.

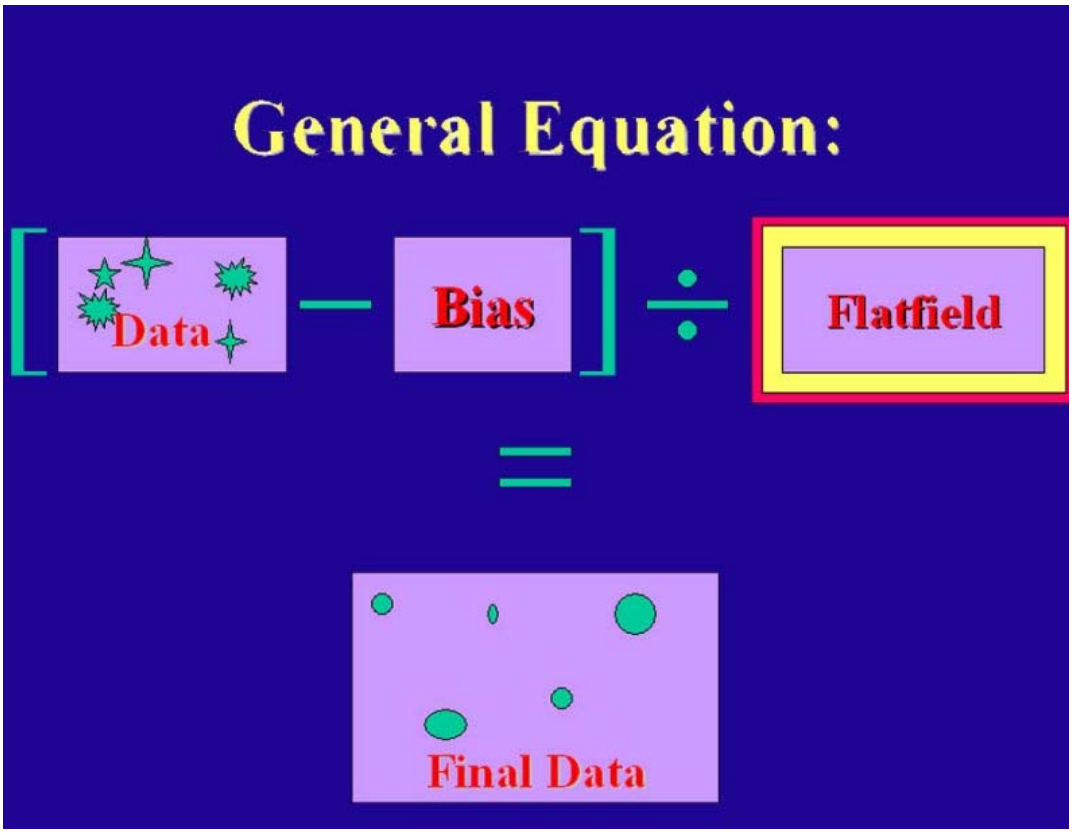

Figure 7: General Equation Followed to Convert Raw Data Into Final Data

Due to the coarse wavelength spacing used to obtain the flatfield measurements, there were too few flatfield measurements to work with. As a result, these flatfield images, spread out over 50 nm intervals as shown in Figure 8, were divided into the difference of the raw data and bias in order to get accurate final data measurements at wavelengths throughout the visible color spectrum. This method turned out to be very inaccurate as calculations were applied inappropriately using only wavelengths measured in the observatory.

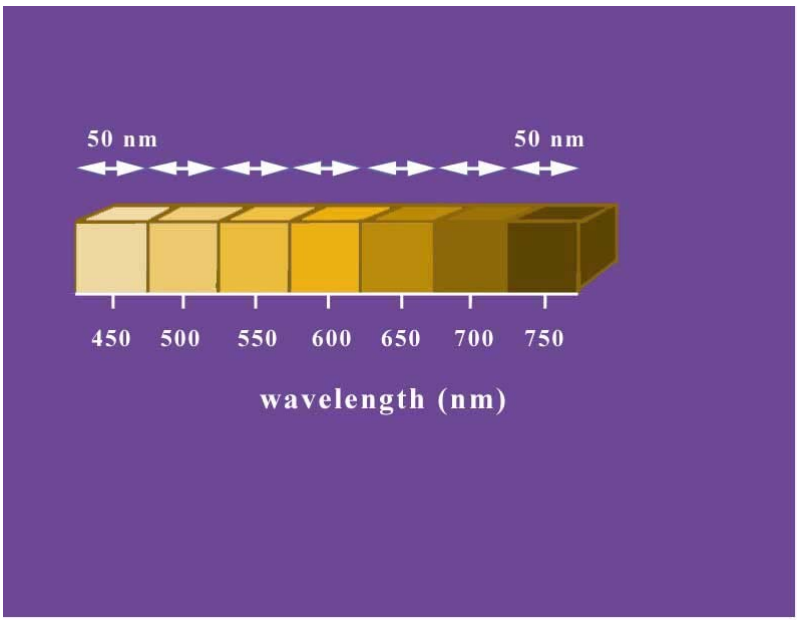

Figure 8: Flatfield Spread diagram for original measurements

Taking this flatfield spread into account and the fact that the different sensitivity variances were not taken into consideration, the original results were not optimal. The team set up a laboratory simulation of the observatory as an optimal system by surrounding the filter of the original imaging system with a white background to recreate the conditions at the Las Campanas Observatory at the time of the original mesaurements. Slawson was then able to compile the new and more accurate sensitivity variance (flatfield) measurements for our project using wavelength intervals of fifteen nanometers rather than fifty nanometers. As a result, more accurate final spectral energy distributions were produced.

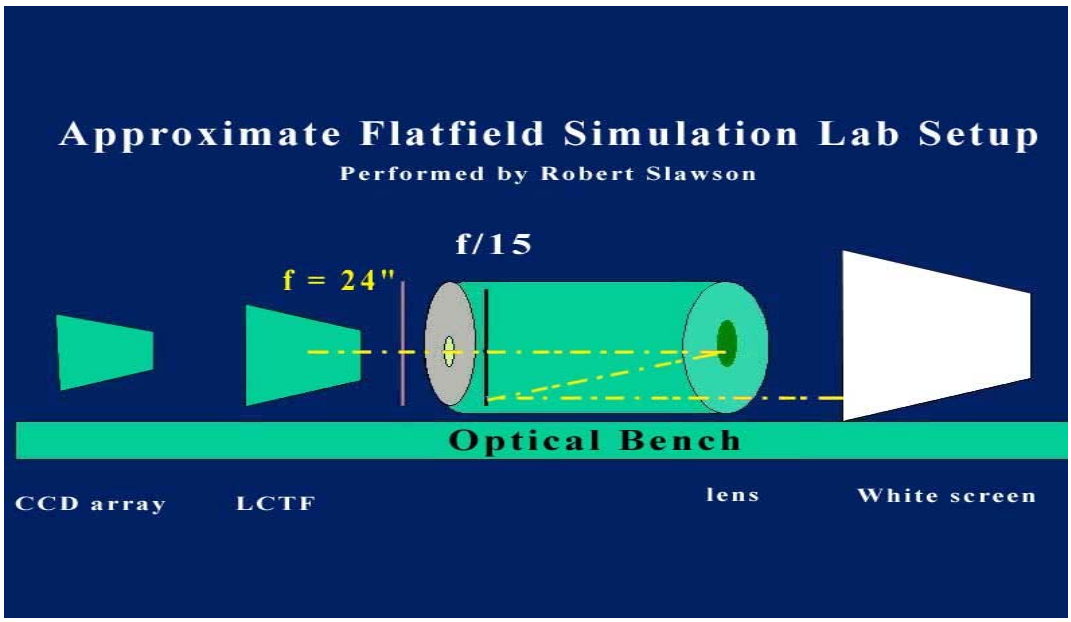

Figure 9: Approximate Flatfield Simulation Lab Setup courtesy of Robert Slawson

Using the resulting measurements of the new flatfield compilation technique for the experimental tunable liquid-crystal filter, I focused on four stars, all classified as type B1-V in the literature. These spectra were Star 2 of Quadrant II, I-13 of Quadrant I, III-7 of Quadrant III and IV-14 of Quadrant IV. My role was to test how much of an improvement the new flatfield measurements made compared to the old flatfield measurements. In order to do this, I took six different types of stellar graphs from the Gunn & Stryker[2] atlas look up tables – 08F, 06, B1-V, B-V, B2-V and B3-V (Figure 10).

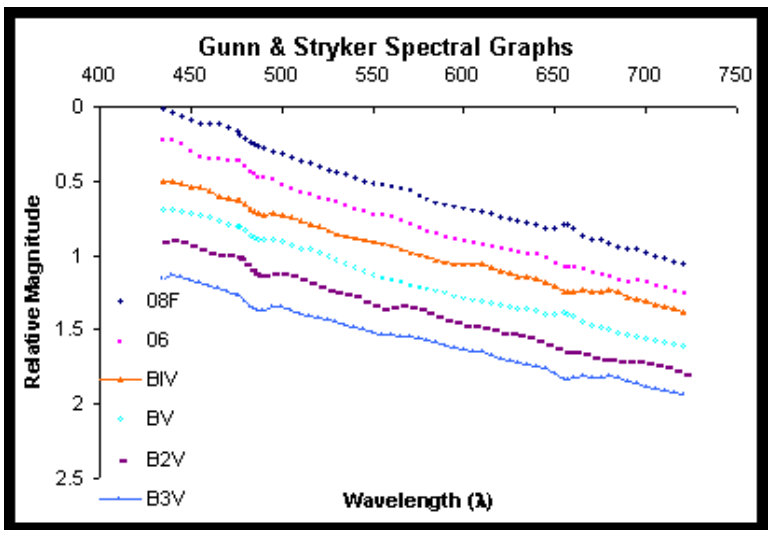

Figure 10: Gunn & Stryker Atlas of Six Spectral Types

The four test spectra from the Jewel Box cluster were fitted to each of the above six Gunn & Stryker[2] spectra using the Root Mean Square (RMS) Error equation (Equation 1) in order to find which of the six Gunn & Stryker[2] spectra the four unknowns were closest in spectral characteristics to. Sigma squared, σ^2, was calculated using the experimental magnitude captured by the filter imaging system. The reference (ref) and experimental (exp) values denoted with the subscript i accounted for the magnitude at wavelength i.

Equation 1: Root Mean Square Error :

$$\left[\frac{\sum_i \frac{1}{\sigma_i^2}(ref_i - \exp_i)^2}{\sum \frac{1}{\sigma_i^2}}\right]^2$$

From there, the team could make an estimate as to which of the spectral types our four unknown stars from the Jewel Box cluster fit based on the lowest Root Mean Square Error. Once the estimates are made as to the spectral type of the star, we can see if our filter system worked successfully by comparing our estimates with the published work of Arp and Van Sant (1958)[3].

Results:

The Gunn & Stryker atlas spectral types were compared with the final data obtained using the old and new flatfield measurements. The graphs for each of the six Gunn & Stryker spectral atlas fits together with the four stars in the field were plotted. In Figure 11, the old and new spectral energy distributions for Star III-7 from Quadrant III of the Jewel Box Cluster is compared with the Gunn & Stryker[2] spectral types 08F, 06, B1-V, B-V, B2-V and B3-V atlas values to see which comparison has the least Root Mean Square Error. This would in turn indicate a strong similarity between the two spectral types – known (Gunn & Stryker) and unknown (Star III-7). The red and turquoise blue plots are the atlas value (reference) while the magenta plot is the old flatfield result and the dark blue plot is the new flatfield result. As the graph shows, there is a closer fit between the new flatfield results and the spectral type. Given this visual graph, the RMS
Error value is higher for the old measurements and lower for the new measurements is almost guaranteed.

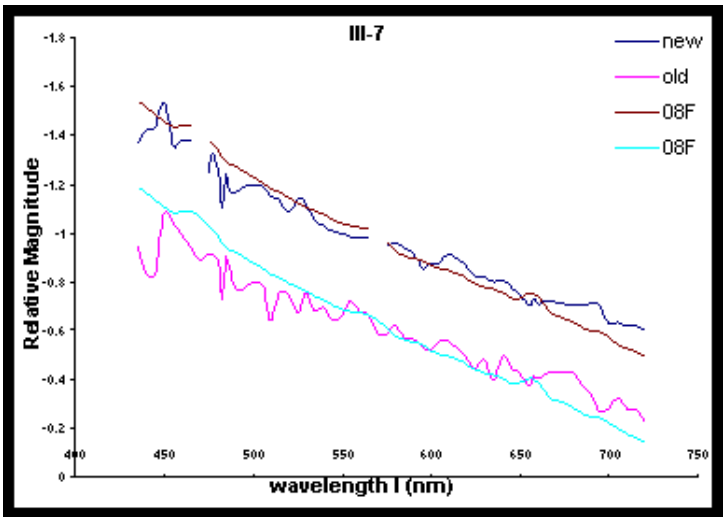
III-7
new
old
08F
08F
Relative Magnitude
wavelength l (nm)

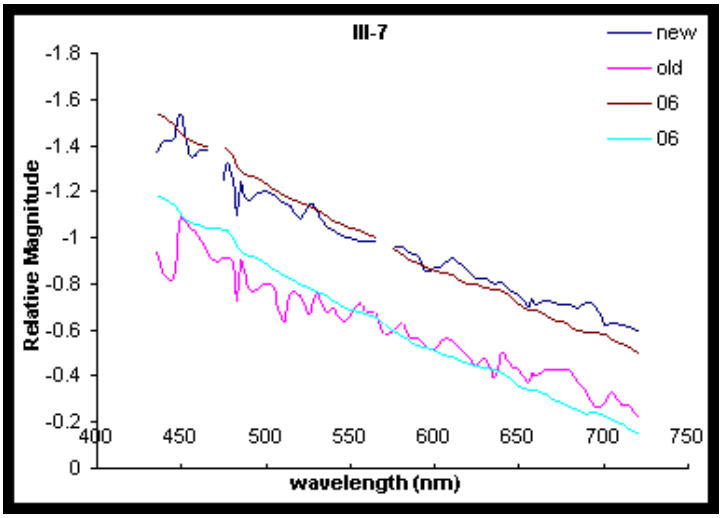
III-7
new
old
06
06
Relative Magnitude
wavelength (nm)

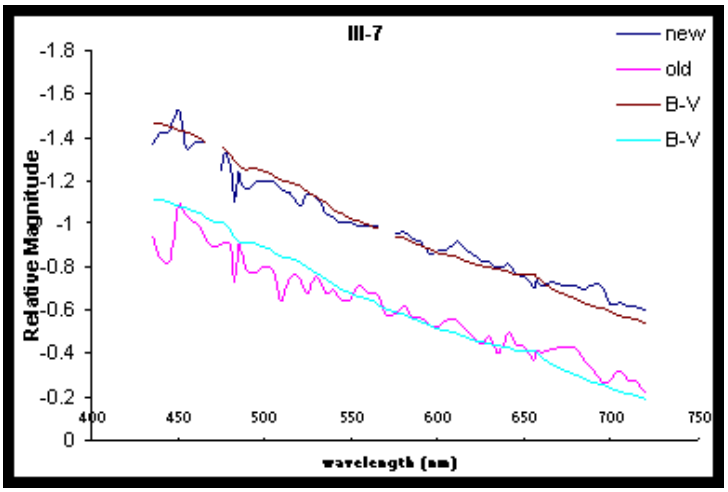
III-7
new
old
B-V
B-V
Relative Magnitude
wavelength (nm)

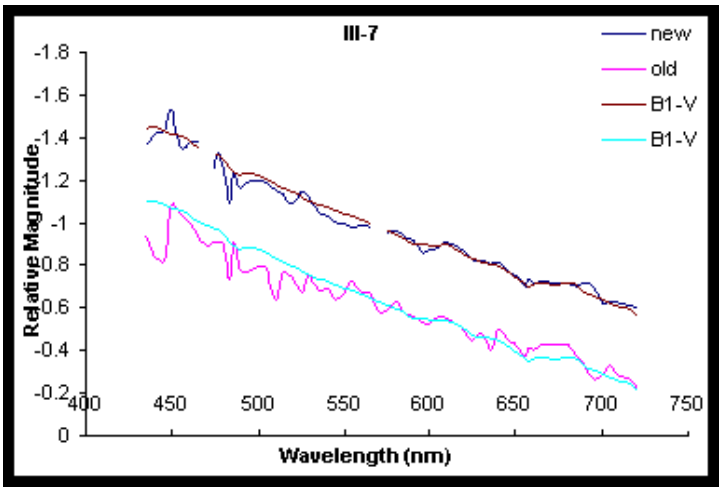

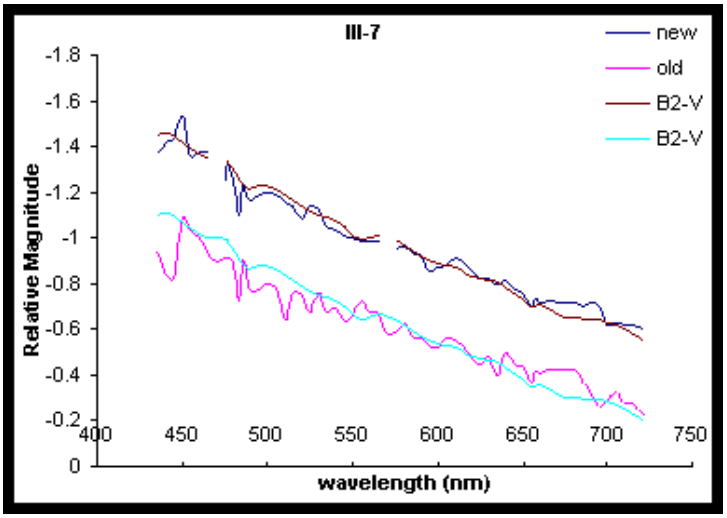

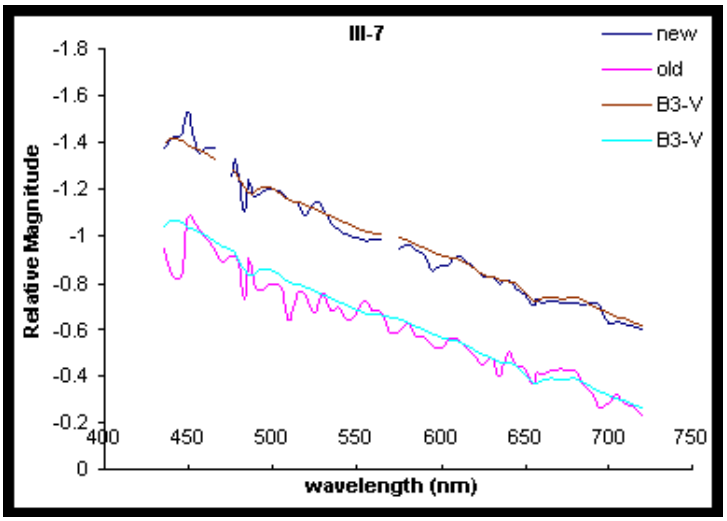

Figure 11: Example of graphical fit comparisons for Star III-7 original and final data sets with Gunn & Stryker[2] six reference stars

From these graphs in Figure 11, we can see by eye that III-7's characteristics have a strong correlation with stars

between spectral types B1-V and B3-V. To quantify this conclusion, we need to calculate the RMS Error, the correlation of the stars' spectrum with the Gunn & Stryker stars.

In this case, the objective is to find which graphs – old or new calculations – fit closest with any of the spectral types from the Gunn & Stryker[2] atlas (i.e. the one with the lowest Root Mean Square error is the best fit).

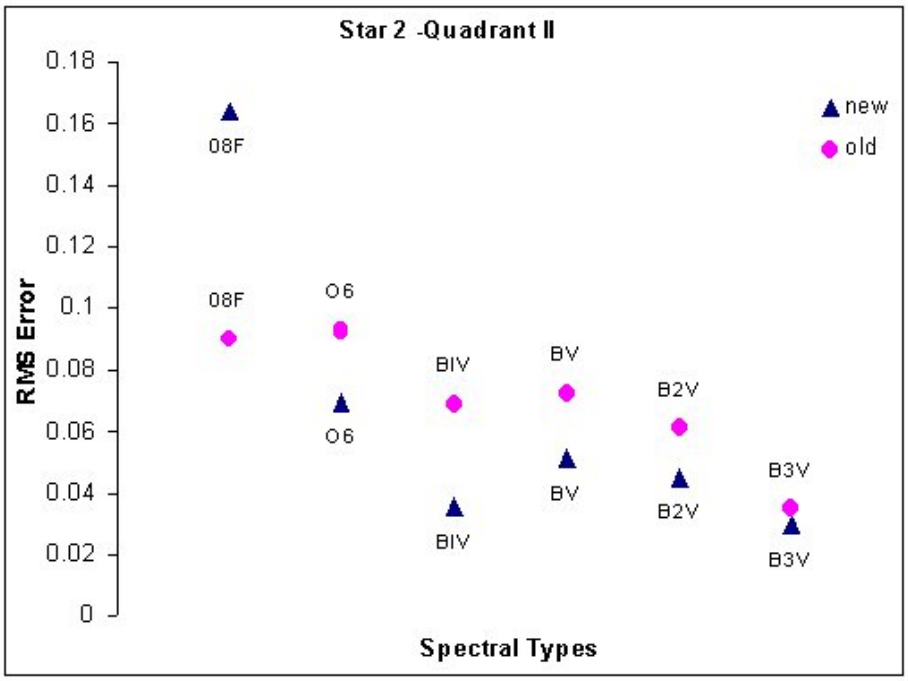

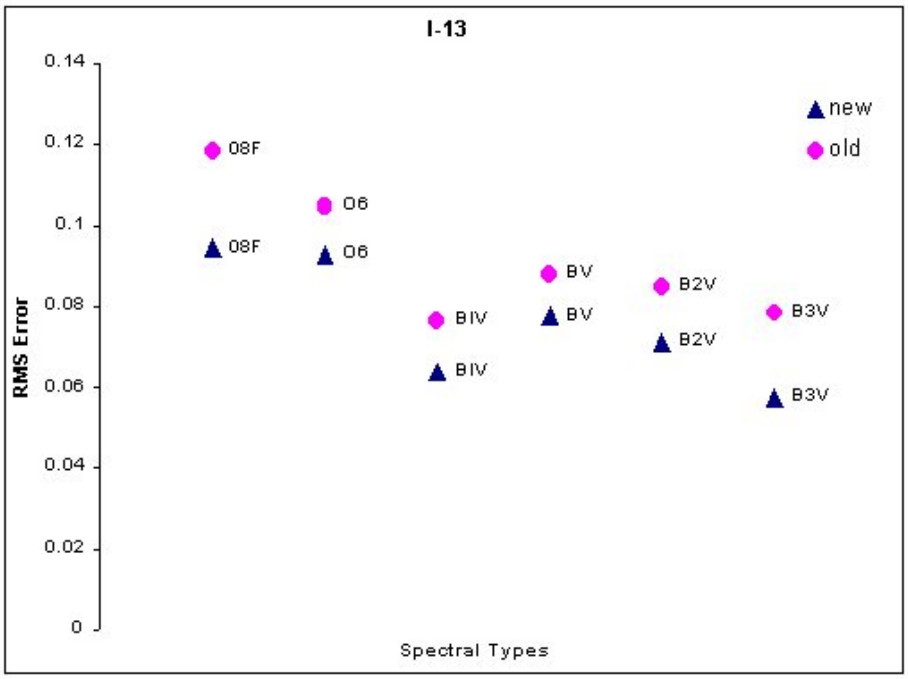

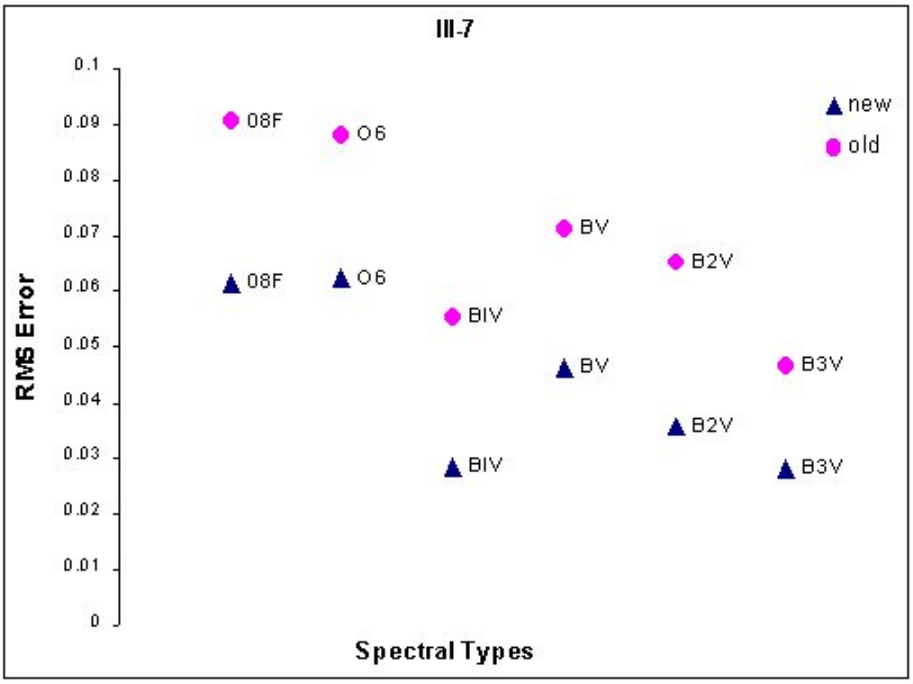

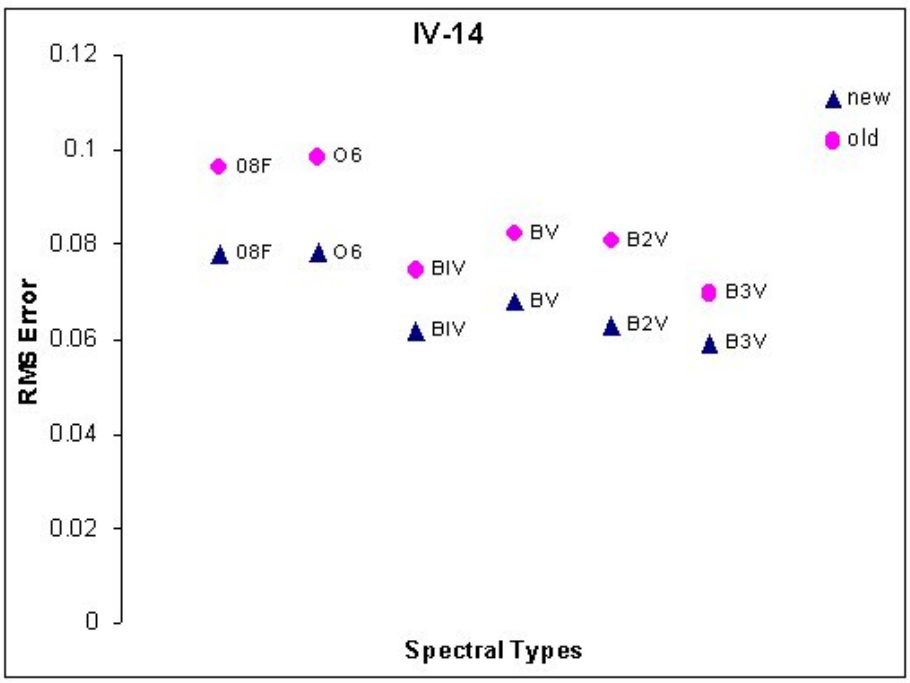

Figure 12: Root Mean Square Error calculations for the four test stars' spectrum from Jewel Box Cluster

From the results shown in Figure 12, there is evidence of a stronger correlation from the low RMS Error for all new values for the four stars and the Gunn & Stryker[2] spectral atlas types B1-V and B3-V. As seen in Figure 10, stars B1-V and B3-V have very similar spectral characteristics, which accounts for the low Root Mean Square Error values for both B1-V and B3-V. All four test stars are classified as type B1-V in the Gunn & Stryker literature.

Conclusions:

The original objective of this Senior Project was to analyze and catalog as many stars in the NGC 4755 Jewel Box cluster as possible. This proved to be difficult because the flat field data obtained to calibrate the frames in the field was not sufficiently accurate. A laboratory simulation was set up and the flatfield measurements were re-done in smaller wavelength increments in order to study the stellar data obtained from the observatory with more accuracy.

After the simulation was completed and the new flatfield data applied to the stellar information already on hand, the new data set obtained was used to check for the validity of the new flatfield measurements. Given the data obtained with a comparison with the reference stars from the Gunn & Stryker[2] atlas along with Arp and Van Sant's[3] published works, I was able to confirm that the new flatfield corrections calibrated the data from February 1997's observatory time better than the original flatfield measurements we started with in November of 1999 at the beginning of my involvement with this research project through the use of the Root Mean Square error algorithm.

Table of Contents

References:

1 R.W. Slawson, Z. Ninkov, E.P. Horch, "Hyperspectral Imaging: Wide-Area Spectrophotometry Using A Liquid-Crystal Tunable Filter," Astronomical Society of the Pacific. 759:621-626, (1999).

2 J.E. Gunn & L.L. Stryker, "Stellar Spectrophotometric Atlas, Wavelengths from 3130 to 10800A," Astrophysical Journal Supplemental Series 52:121-153(1983)

3 H.C. Arp & C.T. Van Sant, "Southern Hemisphere Photometry 1. Photoelectrically-Measured Extinction," Astronomical Journal 63:58(1958)

4 B.F. Lyot, "Patent # 2718170 Slitless Spectrophotometer," Official Gazette of the United States Patent Office 698:386(1955)

Table of Contents

Astronomical Hyperspectral Imaging

Katherine Hoheusle

Symbols:

Symbol/Abbreviation	Definition
nm	**Nanometers ($1x10^{-9}$ meters)**
μm	**Micrometer ($1x10^{-6}$ meters)**
cm	**Centimeter (10×10^{-3} meters)**
σ^2	**Variance**
RMS	**Root Mean Squared**

Table of Contents